atoms

MDPI

Review

Microcalorimeters for X-Ray Spectroscopy of Highly Charged Ions at Storage Rings

Saskia Kraft-Bermuth [1,*], Daniel Hengstler [2], Peter Egelhof [3,4], Christian Enss [2], Andreas Fleischmann [2], Michael Keller [2] and Thomas Stöhlker [3], for the SPARC collaboration

1 I.Physics Institute, Justus-Liebig-University, 35392 Giessen, Germany
2 Kirchhoff Institute, Heidelberg University, 69120 Heidelberg, Germany; Daniel.Hengstler@kip.uni-heidelberg.de (D.H.); enss@kip.uni-heidelberg.de (C.E.); andreas.fleischmann@kip.uni-heidelberg.de (A.F.); michael.keller@kip.uni-heidelberg.de (M.K.)
3 GSI Helmholtz Centre for Heavy Ion Research, 64291 Darmstadt, Germany; p.egelhof@gsi.de (P.E.); t.stoehlker@gsi.de (T.S.)
4 Institute of Physics, Johannes Gutenberg University, 55128 Mainz, Germany
* Correspondence: saskia.kraft-bermuth@iamp.physik.uni-giessen.de; Tel.: +49-641-9915202

Received: 25 January 2018; Accepted: 26 October 2018; Published: 2 November 2018

Abstract: X-ray spectroscopy of highly charged heavy ions is an important tool for the investigation of many topics in atomic physics. Such highly charged ions, in particular hydrogen-like uranium, are investigated at heavy ion storage rings, where high charge states can be produced in large quantities, stored for long times and cooled to low momentum spread of the ion beam. One prominent example is the determination of the 1s Lamb Shift in hydrogen-like heavy ions, which has been investigated at the Experimental Storage Ring (ESR) at the GSI Helmholtz Centre for Heavy Ion Research. Due to the large electron binding energies, the energies of the corresponding photon transitions are located in the X-ray regime. To determine the transition energies with high accuracy, highly resolving X-ray spectrometers are needed. One concept of such spectrometers is the concept of microcalorimeters, which, in contrast to semiconductor detectors, uses the detection of heat rather than charge to detect energy. Such detectors have been developed and successfully applied in experiments at the ESR. For experiments at the Facility for Antiproton and Ion Research (FAIR), the Stored Particles and Atoms Collaboration (SPARC) pursues the development of new microcalorimeter concepts and larger detector arrays. Next to fundamental investigations on quantum electrodynamics such as the 1s Lamb Shift or electron–electron interactions in two- and three-electron systems, X-ray spectroscopy may be extended towards nuclear physics investigations like the determination of nuclear charge radii.

Keywords: storage rings; high-precision x-ray spectroscopy; highly charged ions; microcalorimeters

PACS: 32.30.Rj; 7.20.Mc; 7.85.Nc

1. Introduction

High-precision X-ray spectroscopy of highly charged ions has provided important input in many fields of physics. A prominent example is astrophysics, where the identification of X-ray lines emitted by highly charged ions, starting with oxygen and expanding up to iron and even higher nuclear charges, has become important for the interpretation of astrophysical spectra [1]. Concerning quantum physics, the test of the theory of quantum electrodynamics (QED) is another outstanding issue. While QED has been evaluated and experimentally tested extensively for hydrogen [2,3], its investigation in the very high Coulomb fields around nuclei with high nuclear charge is still falling behind in calculational and experimental accuracy. On the other hand, the precise determination of the Lamb

Shift of the 1s and the $2s_{1/2}$ state in hydrogen-like ions of high nuclear charge Z is an important tool for the investigation of QED in very strong Coulomb fields, both in theory [4–6] and experiment [7–10]. Experiments aim at the precise determination of the transition energies from $n \geq 2$ to $n = 1$ states, commonly denoted as *Lyman transitions*. Furthermore, the corresponding transitions in helium- or lithium-like ions may provide information on electron–electron-interaction. For ions of high Z, these transitions lie in the X-ray regime.

The aforementioned astrophysics or QED experiments have become possible only after ions in high charge states became available in sufficient quantities under well controlled experimental conditions. In fact, the first Electron Beam Ion Trap (EBIT-I) at the Lawrence Livermore National Laboratory was primarily designed as an X-ray source for spectroscopy. This machine and its successors EBIT-II and SuperEBIT have produced a wealth of data for astrophysics, atomic physics, fusion and other fields [11–13]. Thereby, the SuperEBIT has obtained highest charge states also for very heavy ions up to helium-like uranium [14]. The most precise determination of electron transition energies for lithium-like uranium was performed at the SuperEBIT by Beiersdorfer et al. with an accuracy of 5×10^{-5} [15].

However, if hydrogen-like ions are considered, even the SuperEBIT can only provide very small quantities [16,17]. Accordingly, experiments on hydrogen-like very heavy ions are currently mostly performed at heavy ion accelerators. Among them, heavy ion storage rings offer the unique possibility of accumulating and cooling the ions. In particular, the Experimental Storage Ring (ESR) at the GSI Helmholtz Centre for Heavy Ion Research is presently the only storage ring worldwide which provides all ions and charge states up to bare uranium in a wide energy range from 500 MeV/u down to about 4 MeV/u [18]. The interaction with an electron beam cools the ion beam to a momentum spread of $\Delta p/p \leq 10^{-4}$ [19]. Among the rich variety of experiments performed at the ESR, the determination of the 1s Lamb Shift of hydrogen-like heaviest ions stands out as a high-precision X-ray experiment. The 1s Lamb Shift of hydrogen-like uranium was determined at the ESR electron cooler by Gumberidze et al. with an accuracy of 1% [19]. Presently, the experimental storage facilities at GSI are extended by the installation of the CRYRING, a second storage ring which operates at energies down to $\leq$300 keV/u [20], and the installation of the HITRAP facility where the ions will be captured in a Penning trap and cooled to ion temperatures of about 4 K [21,22]. These three facilities will be connected, thus providing a versatile experimental area not only for stable ions, but—in connection with the fragment separator FRS [23]—also for unstable nuclides. CRYRING is already a part of the Facility for Antiproton and Ion Research (FAIR) [24] which is currently under construction at Darmstadt. The combination of ESR, CRYRING and HITRAP will be complemented on the high-energy side by the High-Energy Storage Ring (HESR) [25], which is part of the FAIR project and which will extend the energy range towards high energies up to a few GeV/u. In this energy range, new effects of ions interacting with photons or electrons are expected [26]. An overview of the existing and future storage facilites at GSI and FAIR is given in Figure 1.

Next to experimental facilities which provide high-Z ions with sufficient intensities, high-resolution X-ray detectors are mandatory for a precise determination of X-ray transition energies as well as for the identification of close-spaced X-ray lines in the spectra. Among the different detector concepts, two have been widely applied for X-rays in the energy range of 1–150 keV.

High-resolution germanium detectors combine a relatively good energy resolution with large detector solid angle and, therefore, with high detection efficiency. They have been and are still widely used with excellent results, for example at the Livermore EBIT [12] and at the ESR [19,27]. However, for X-ray energies below 100 keV, they reach inherent limitations in energy resolution of around $\Delta E/E \sim 10^{-2}$. In germanium detectors, the energy of the incoming photon creates electron-hole-pairs and is detected as a voltage signal which is proportional to the number of the created charges. As a consequence, the resolving power $E/\Delta E$ is proportional to the square-root of the number of created charges. As this number drops for low X-ray energies due to the finite excitation energy of around 1 eV in germanium, the resolving power decreases.

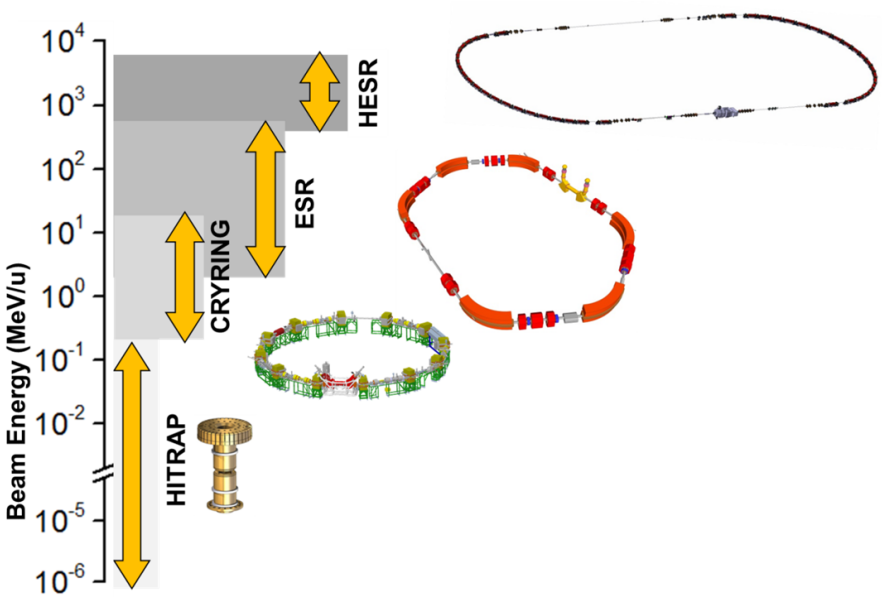

Figure 1. An overview of the storage facilities for highly charged ions of GSI and FAIR with their respective energy ranges is displayed. Stable ions as well as unstable nuclides are injected into the Experimental Storage Ring (ESR) [18] where they are stored, cooled by the interaction with an electron beam, and decelerated to the energy desired for a specific experiment. The ESR is connected to the low-energy storage ring CRYRING [20]. In the CRYRING, the ions may be stored and cooled at a maximum energy of 14 MeV/u or further decelerated. From the CRYRING, a transfer beam line leads to the HITRAP facility [21,22] where the ions are loaded into a Penning trap and cooled to a kinetic energy corresponding to about 4 K. On the high-energy side, stable and unstable nuclides will be injected into the High Energy Storage Ring (HESR) at the FAIR facility [25]. All storage facilities are or will be equipped with several experimental installations, including a transverse gas-jet target and a facility for laser spectroscopy. This figure was reprinted from [26] (used by permission).

Crystal spectrometers use the dispersion of X-rays in a silicon crystal in combination with a position-sensitive detector. Several of these crystal spectrometers are in use at EBITs at Livermore [11,12], Heidelberg [28,29] or others [30,31]. Excellent energy resolution of $\Delta E/E \sim 10^{-3} - 10^{-4}$ has been obtained in the energy range of 1–30 keV. At the ESR, the X-ray spectrometer FOCAL (FOcusing Compensated Asymmetric Laue) [32] has been developed for X-ray energies around 70 keV, optimized for experiments on the 1s Lamb Shift of hydrogen-like ions. For these high X-ray energies, FOCAL obtains an excellent energy resolution of $\Delta E/E \sim 10^{-3}$. It has recently been applied successfully in an experiment on the 1s Lamb Shift of hydrogen-like gold [32]. Notwithstanding their very successful application, crystal spectrometers are also subject to limitations. The dynamic range is limited by the Bragg condition to a relatively small energy range around a central X-ray energy value. The use of diffraction crystals of different sizes or different geometries solves this problem to a certain extent, but it may introduce systematic errors when comparing different measurements (for a more detailed discussion see [31] and the references cited therein). In addition, crystal spectrometers pay for their excellent energy resolution with a rather low detection efficiency which drops considerably for X-ray energies above 30 keV. For example, the FOCAL spectrometer obtains a crystal efficiency of $2 \times 3 \times 10^{-8}$ at an X-ray energy of 60 keV [32].

Microcalorimeters provide a third, alternative detector concept. Such devices detect photons by an increase in temperature rather than by a creation of charges. As the excitation energy of a phonon is of the order of 1 meV as compared to 1 eV for ionization in a germanium or silicon detector, a given amount of energy creates about a factor of 1000 more phonons than electron-hole-pairs. This higher number of quanta allows for an improvement in energy resolution by about one order of magnitude. Accordingly, the detection principle of microcalorimeters provides a large dynamic range

like a germanium detector while maintaining an excellent energy resolution comparable to the energy resolution obtained by crystal spectrometers. In addition, the combination of single microcalorimeters into arrays of hundred or more single pixels allows for the realization of relatively large detector solid angles. In terms of detection efficiency, this feature places microcalorimeters between germanium detectors with their large active detector areas and crystal spectrometers with their rather small angular acceptance. In [33], Uhlig et al. have given an extensive comparison of microcalorimeters and crystal spectrometers with respect to energy resolution and detection efficiency. Although the discussion focuses on X-ray energies below 10 keV, the same arguments apply for microcalorimeters for high X-ray energies as presented here.

The application of microcalorimeters for high-precision X-ray spectroscopy at the ESR to investigate the 1s Lamb Shift in hydrogen-like heavy ions was proposed by Egelhof et al. in 1996 [34]. Aside from systematic uncertainties connected to the high energies of the ions in the storage ring, i.e., the correction of the Doppler shift, the energy resolution of the germanium X-ray detectors is one current limitation of the accuracy of these investigations. Therefore, applying microcalorimeters may eventually improve the accuracy of the 1s Lamb Shift in hydrogen-like heavy ions below the 1% which is the current state-of-the-art [19]. A first attempt with germanium microcalorimeters was made in 2003 [35]. It showed that it was necessary to develop a microcalorimeter setup which is adapted to the specific experimental conditions at the ESR. As a consequence, two microcalorimeter systems have been developed for application at the ESR. Both systems have been applied succesfully at the ESR for high-precision X-ray spectroscopy in the last years. Both approaches have demonstrated an excellent energy resolution of $\Delta E/E \leq 10^{-3}$ in combination with a large dynamic range covering X-ray energies of about 1 to 100 keV. This review summarizes the results of these developments, which have been published in different articles over the years. The aim is to give a concise overview of the status of the two microcalorimeter systems *SiM-X* and *maXs* which have been designed specifically for application at the GSI and FAIR storage rings. One focus of this application is the direct determination of the 1s Lamb shift in hydrogen-like heavy ions, but other experimental foci may evolve with the availability of this new, high-resolution technique.

The article will introduce the detection principle and present the technical realization in Section 2. First results of the application at the ESR will be presented in Section 3. Conclusions and perspectives for future experiments will be given in Section 4.

2. Experimental Setup

2.1. Detection Principle

A scheme of the detection principle of a microcalorimeter is displayed in Figure 2. Such a detector consists of a piece of material which serves as an absorber with a certain heat capacity C. If a particle or photon deposits its kinetic energy E in the absorber, it excites phonons or excitons which decay into phonons after a certain recombination time. After a thermalization time, thermal equilibrium in the absorber is established and the temperature has changed by an amount $\Delta T = E/C$. The absorber is coupled to a thermometer which monitors this temperature rise. The thermal energy is then transferred to a heat sink via a defined thermal link with a thermal conductance G. After cooling down again to the operating temperature, the absorber can detect the next photon. Microcalorimeters are, therefore, single-photon detectors. This distinguishes them from bolometers which detect an integrated photon flux.

The absorber material can be chosen rather freely because the excitation energy of phonons is almost independent of material properties. In particular for X-ray detectors, materials with high nuclear charge Z can be chosen to realize a high detection efficiency. However, to obtain a sufficiently

large temperature signal ΔT, a small heat capacity C of the absorber is mandatory. In general, the heat capacity of most materials is given by the expression

$$C(T) = \gamma \cdot T + \delta \cdot \left(\frac{T}{\Theta_D}\right)^3, \quad (1)$$

where Θ_D is the Debye temperature and γ and δ are material constants. This means that microcalorimeters are usually operated at very low operation temperatures of 100 mK or below. In addition, they may take advantage of using either an insulator or a superconductor as absorber, thereby suppressing the electron heat capacity ($\gamma = 0$). This allows for obtaining very low heat capacities of the order of picojoule per kelvin for X-ray detectors.

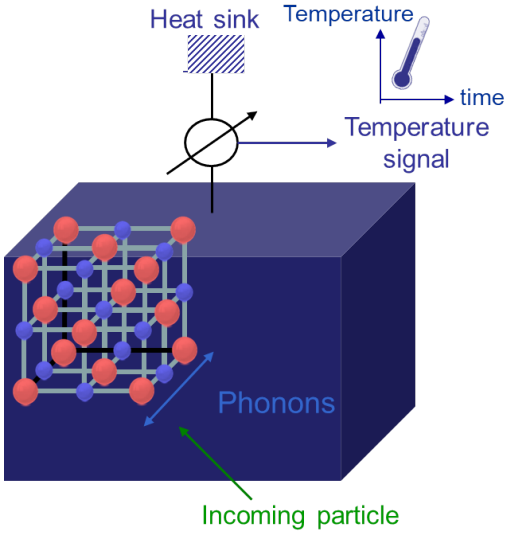

Figure 2. A microcalorimeter consists of an absorber which changes its temperature when an incoming particle excites phonons. A defined coupling to a heat sink drives the absorber back to its original operating temperature. The temperature change is determined by a temperature-dependent resistance or a temperature-dependent magnetization. To obtain high sensitivity, these devices need to be operated at very low temperatures.

The readout of the temperature change ΔT is realized either by a temperature-dependent resistance $R(T)$, or by a temperature-dependent magnetization $M(T)$. Other thermometer technologies include the use of a temperature-dependent inductance [36,37] or the use of superconducting tunnel junctions [38,39]. For each application, the combination of absorber, thermometer and thermal coupling may be optimized. Microcalorimeters of different designs are nowadays applied in many different fields of research, covering X-ray astronomy, infrared astronomy, dark matter research and the detection of alpha particles and heavy ions. An overview of the different types of microcalorimeters and their applications can be found in [40–42].

2.2. Silicon Microcalorimeters

2.2.1. Working Principle of Resistance Thermometers

For the readout of the temperature signal, temperature-dependent resistances are the thermometer type with the longest standing history of development. As the temperature change ΔT is converted into

a resistance change ΔR, a large temperature dependence dR/dT is a prerequisite for high sensitivity. A commonly used figure of merit to characterize resistance thermistors is the parameter

$$\alpha = \frac{T}{R}\frac{dR}{dT}. \quad (2)$$

Nowadays, two basic types of resistance thermometers are applied for X-ray spectroscopy. The largest temperature dependence α can be obtained if a superconductor is stablized in its transition from the normal to the superconducting state. Such Transition Edge Sensors (TES's) obtain large values of $\alpha = 50 - 100$. X-ray detectors with excellent performance have been developed using TES's and are applied with great success in many experiments. For an overview, we refer the reader to the proceedings of the 16th Workshop on Low Temperature Detectors (LTD 16) [41] and the references given therein. A more recent review focused on beamline and laboratory physics can be found in [42,43], where the new TES spectrometer at the EBIT of the National Institute of Standards and Technology (NIST) and the new TEMS spectrometer for the EBIT at the LLNL are discussed.

While X-ray detectors using TES's obtain an excellent energy resolution and fast readout speed, they have one drawback. Their dynamic range is limited to the width of the transition, which is of the order of 1 mK dependent on the TES design. In addition, the low resistivity of the superconducting film usually demands for the readout by a Superconducting Quantum Interference Device (SQUID). As an alternative, the concept of compensated-doped semiconductors has been pursued in parallel. If donor and acceptor doping concentration are chosen as almost equal, at low temperatures, the semiconductor behaves like a so-called Mott insulator [44] with an exponential dependence of the resistance on the temperature. This exponential behaviour allows for a large dynamic range, which is a considerable advantage even though the parameter α is generally more than one order of magnitude lower, $\alpha = 1 - 5$. In addition, the readout electronics of such compensated-doped semiconductors do not involve SQUIDs but can be realized with adapted voltage-sensitive amplifiers at room temperature. Their main disadvantage is the relatively long signal decay time of several hundred milliseconds, which limits the tolerable count rate to several Hertz. However, for many applications in precision spectroscopy, the tolerable count rate is not a serious limitation. Accordingly, compensated-doped silicon thermistors have been applied in a wide variety of X-ray detection experiments. Next to various satellite and balloon missions [45–48], the XRS spectrometer [49] and its successor ECS [50] are deployed at the EBIT and SuperEBIT of the Lawrence Livermore National Laboratory [12]. Both microcalorimeter arrays have produced outstanding X-ray reference data for astrophysics [1,51,52]. Other applications include high-resolution spectroscopy of xenon [53] and praseodymium [54] for QED tests, spectroscopy on tungsten for fusion research [55] and the investigation of X-ray transitions in thorium-229 for the development of an atomic clock [56]. The astrophysics experiments were mostly focused on X-ray energies below 5 keV, while the measurements for xenon [53], praseodymium [54] and thorium [56] were centered around 30–40 keV.

2.2.2. Silicon Microcalorimeters for Hard X-rays

To address the 1s Lamb Shift in hydrogen-like uranium, X-ray energies of up to 120 keV need to be detected with high quantum efficiency. The dynamic range of a semiconductor thermistor itself has only an upper limit where the Mott conductivity breaks down. However, the dynamic range of the whole microcalorimeter is mainly limited by the size of its X-ray absorber. The X-ray energy of 50–100 keV demands for absorbers with high Z and a certain minimum thickness to realize a sufficiently high quantum efficiency. On the other hand, the heat capacity of the absorber has to be kept small in order to maintain a high signal-to-noise ratio. Accordingly, the absorber volume is a compromise between these two contradicting issues. For a TES, the width of the transition poses an additional limit of the dynamic range because the temperature change $\Delta T = E/C$ has to be kept within the transition range.

When Egelhof et al. started to investigate the use of microcalorimeters for Lamb Shift experiments at the ESR, they decided to use silicon microcalorimeters to have a large dynamic range at their disposal [34]. TES thermistors had not yet been combined with thick absorbers at that time. Only in the last few years, TES microcalorimeters for X-ray energies around 100 keV have been developed, mainly for application in nuclear safeguards [43,57,58]. These TES microcalorimeters obtain an excellent energy resolution of 40–50 eV at 100 keV. Their application at an accelerator facility has not been investigated so far, but they have the potential to provide an alternative thermistor concept, in particular for large, multiplexed detector arrays.

The silicon thermistor arrays were developed and fabricated by Stahle et al. primarily for balloon and satellite missions with astrophysical interest [45,46]. They consist of two rows of eighteen silicon pixels which are micromachined from a full silicon wafer. The thermistor is formed by an area which is compensated doped by phosphorus and boron.

The silicon thermistors for ESR experiments were equipped with absorbers of lead (thickness 50 μm) or tin (thickness 100 μm) [59,60]. Thus, the quantum efficiency obtained for 100 keV X-rays is around 20%. The active area per pixel is around 0.35 mm^2. For a fully equipped detector array with 32 pixels, this amounts to an active detector area of 11 mm^2. The thermal decay constant of around 1 ms at the operating temperature of 50 mK permits count rates of around 1 Hz without the need for pile-up correction. Figure 3 displays the layout of one pixel [46], one of the detector arrays used in the ESR experiments [60] and a close-up where the tin and lead absorbers are visible. The cryogenic setup is discussed in the next section.

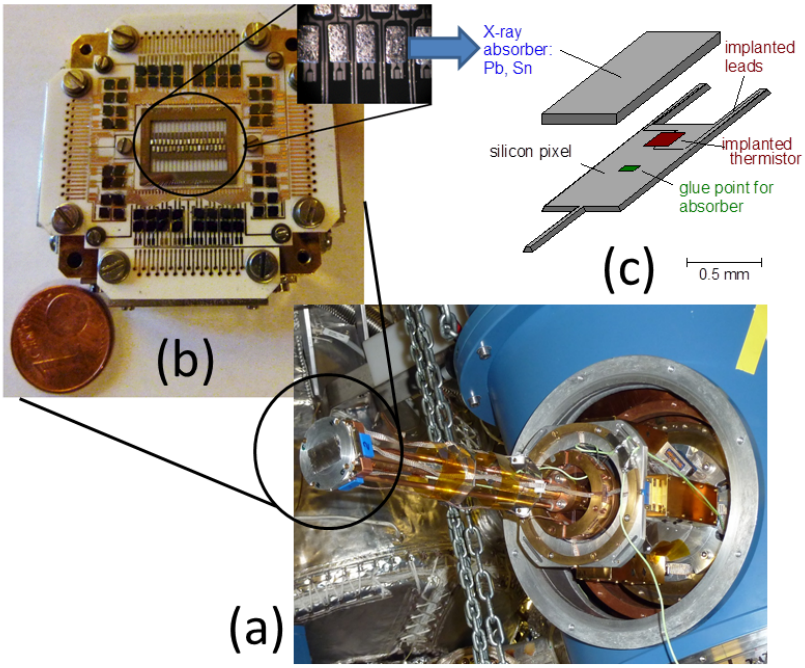

Figure 3. (color online) (**a**) the lower right photograph shows the side arm of the cryostat with the detector array mounted at its end (the array is protected by an aluminum cover with a thin aluminum foil); (**b**) the upper left photograph shows the detector array equipped with Sn absorbers; (**c**) next to it, a schematic of one single detector pixel is displayed [46,60,61].

The detector pixels were characterized in the laboratory using a ^{241}Am source with a γ-line at about 59.5 keV. An excellent energy resolution of 50–60 eV was obtained for all pixels [60,61]. Figure 4 shows one example of a spectrum with an energy resolution of 46 eV, collected with a tin absorber.

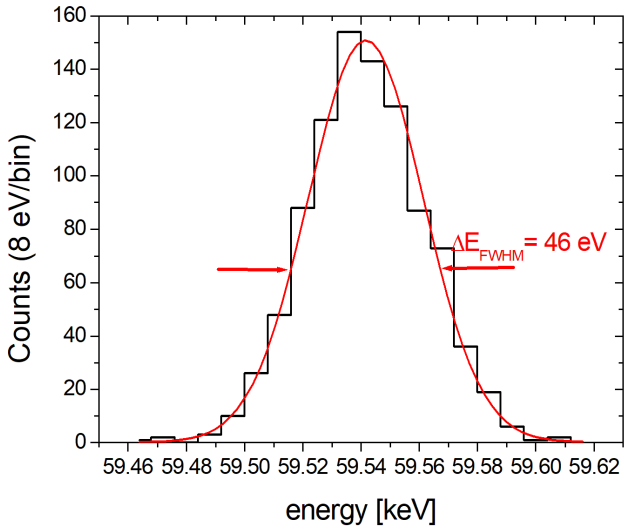

Figure 4. This example spectrum of one silicon microcalorimeter with a tin absorber demonstrates the excellent energy resolution of $\Delta E = 46$ eV at 59.5 keV [61].

2.2.3. Cryogenic Setup

A sufficiently low heat capacity of the absorber and a sufficiently high dR/dT of the thermometer to realize $\Delta E/E \sim 10^{-3}$ for X-ray energies of around 100 keV can only be reached if an operation temperature below 100 mK is maintained. Optimal use of the limited beam time at the ESR as well as the demand for high cooling power at low temperatures defined the use of a ^{3}He/^{4}He dilution refrigerator with a large storage of liquid helium and liquid nitrogen as cooling agents for the outer temperature shields. In the first place, the silicon microcalorimeters were adapted for experiments to determine the 1s Lamb Shift on hydrogen-like heavy ions [7,34]. In such experiments, a beam of bare heavy ions interacts with a jet of molecular gas (nitrogen, argon or xenon). A special gas-jet target is installed at the ESR to provide a high target density without compromising the excellent vacuum which is necessary for storing the ions [62,63]. The cryostat in which the microcalorimeters are operated had to be specially adapted to fit the geometry of this gas-jet target, i.e., to bring the detectors as close as possible to the interaction zone of ion beam and gas-jet, while maintaining the low operating temperature in the cryostat as well as the excellent vacuum in the storage ring. Accordingly, the cryostat was equipped with a side arm of about 600 mm length [60]. The detectors are mounted at the end of a copper rod which in turn is connected to the coldest point of the cryostat at 10 mK. Due to the finite thermal coupling, the detectors themselves are operated at around 50 mK. Figure 3 shows an example of a fully equipped detector array mounted at the cryostat side arm. A detailed description can be found in [34,60,64].

While this cryogenic setup has worked very well at the ESR gas-jet target, it also poses limitations to the flexibility of experiments. In addition, the use of ^{4}He increases the operational costs and demands interruptions of beam time for refilling. Therefore, for the next generation of microcalorimeters, a ^{3}He/^{4}He dilution refrigerator with a pulse tube cooler for the outer temperature shields was designed and commissioned [65]. It features a side arm which is kept at an operating temperature of 10 mK and fits into the ESR gas-jet target like the setup of Bleile et al. [60], but the system does not need any maintenance during beam times. In addition, the design of the inner geometry allows for vertical mounting of the side arm in addition to the horizontal setting. This makes the new cryogenic setup much more flexible and adaptable to different experimental needs.

2.2.4. SiM-X: The Next Generation Silicon Microcalorimeter Array

The two arrays used in the Lamb Shift experiments had an active detector area of 2 mm^2 and 4 mm^2, which resulted in an overall detection efficiency (including solid angle) of 7×10^{-7} and 1.4×10^{-6} under the given experimental conditions at the ESR. The main goal of the next generation silicon microcalorimeter array was to increase this detection efficiency by increasing the active detector area to about 30 mm^2. As the heat capacity limits the active area of one single detector pixel, the number of the detector pixels has to be increased from 12 as of now to 96. On the other hand, the geometrical constraints at the ESR gas-jet target limit the outer diameter of the side arm to 90 mm [60,65]. Accordingly, the mount of the detectors was re-designed by introducing additional high-density plugs in order to fit three detector arrays with a total of 96 pixels inside the vacuum chamber of the side arm (see Figure 5). A prototype setup with one detector array with 32 pixels was constructed and successfully tested at the ESR [66]. The new design is displayed in Figure 6. Since the first test, improvements in the production procedure have led to an energy resolution of 120 eV at an X-ray energy of 60 keV. The energy resolution is currently limited by vibrational noise from the pulse tube. Further improvements in performance are expected by installing effective vibration damping in the cryogenic setup. In parallel, the production of the 96 pixel array is currently in progress.

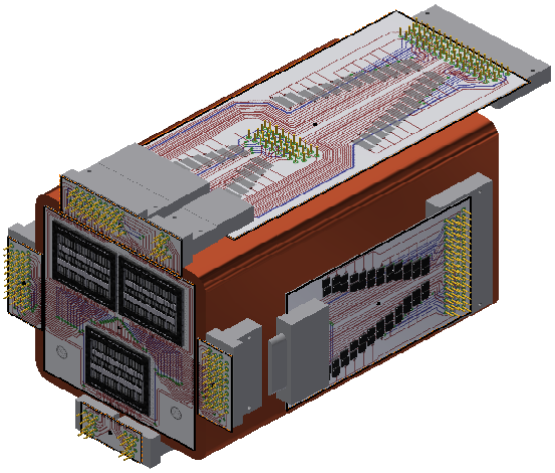

Figure 5. (color online) The schematic shows the design of the new, more compact silicon detector array with 96 pixels [66].

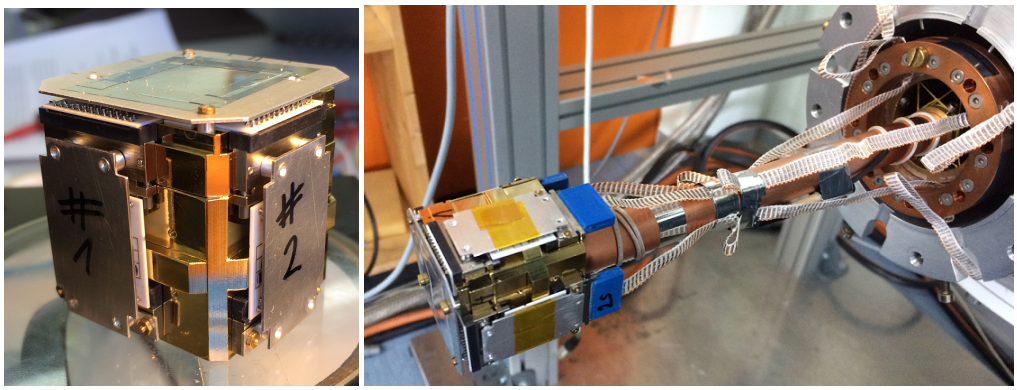

Figure 6. (color online) The prototype of the more compact design features one array with 32 pixels, mounted at the front of the side arm (right-hand side). Pictures courtesy of P. Scholz.

2.3. Metallic Magnetic Calorimeters

2.3.1. Working Principle

Magnetic calorimeters use the Curie-like temperature dependence of the magnetization of a paramagnetic material in a weak magnetic field to precisely determine the temperature change of the detector after the absorption of an X-ray photon [67,68]. The resulting change of magnetization is then read-out by a highly sensitive low-noise SQUID magnetometer as shown in Figure 7. The depicted detector layout makes use of two single pixels that are read out in parallel. This gradiometric setup minimizes the effect of temperature fluctuations of the heat bath and allows the preparation of a superconducting persistent current in the pick-up coil that generates the magnetic field that is required for the temperature sensor. The temperature sensors developed by our group make use of gold or silver that is doped with several hundred ppm of the rare-earth element erbium. The thermodynamic properties of these materials are well understood [69]. As the detectors can be fabricated in our in-house cleanroom, key features of a calorimeter like energy resolution, active detection area and detection efficiency can be optimized and adapted to the needs of a given experiment.

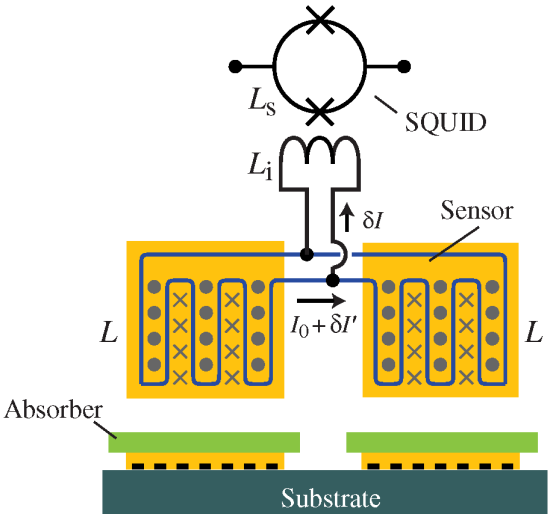

Figure 7. Schematic drawing of a gradiometric detector consisting of two single metallic magnetic calorimeters. A persistent current I_0 in the superconducting coil can be used to generate the weak magnetic field that is needed to operate the paramagnetic temperature sensor. A SQUID magnetometer is used to monitor any additional current δI that arises from a temperature change of one of the detectors after the absorption of a photon.

As was discussed in Section 2.2.1, microcalorimeters with transition edge sensors (TES) obtain excellent energy resolution and energy linearity, but their dynamic range is limited to the transition region. TESs with a saturation energy of 100 keV obtain an excellent energy resolution for this high X-ray energy [43,57,58], but the large absorber size, which is needed for high quantum efficiency but also to reach the high saturation energy, limits their energy resolution for the low X-ray energies. In contrast, magnetic calorimeters do not suffer from an abrupt saturation at the upper end of the acceptance range and can be used over a very wide energy range with the same absorber heat capacity. Additionally, the detector response exhibits an outstanding linearity and the small deviations from the linearity are well understood and can be derived from the thermodynamical properties of the microcalorimeter [70].

Despite the higher specific heat compared to dielectric or superconducting materials and the corresponding smaller signal sizes, our magnetic calorimeters make use of absorbers made of gold. Thereby, they benefit from the very high detection efficiency and especially from the very good thermal conductivity of gold. Furthermore, large arrays benefit from the fact that absorbers made of gold can

be electroplated directly on top of the temperature sensors reliably in a convenient and reproducible way. The high thermal conductivity ensures that the absorber quickly reaches thermal equilibrium after the absorption of a photon, and that no long-living states, as they are observed in insulators, semiconductors and superconductors [71–73], are created. By the metallic glue-less contact to the sensor, which is facilitated by the electroplating process, and the very fast thermalization of the conduction electrons of the metallic sensor with the paramagnetic moments, a very short intrinsic signal rise time of 90 ns can be achieved [74]. Together with the good energy resolution, which is discussed in the following section, metallic magnetic calorimeters offer a great combination of properties that can be of use in various experiments.

2.3.2. The *maXs* Detector Arrays

For the use in X-ray spectroscopy, we developed and fabricated three different general-purpose detector arrays that are optimized for different energy ranges. The detector arrays *maXs-20* and *maXs-200* consist of eight detectors arranged in a one-dimensional line. Both arrays are optimized for X-ray energies up to 20 keV, and 200 keV, respectively, and are discussed in more detail in [75]. In experiments with the *maXs-20* detector, an energy resolution of $\Delta E_{\mathrm{FWHM}} = 1.6$ eV at 6 keV was achieved for an individual detector channel [76]. With an absorption efficiency above 75% for energies around 100 keV and an energy resolution of $\Delta E_{\mathrm{FWHM}} = 46$ eV at 60 keV [70] the *maXs-200* detector is very well suited for spectroscopic studies of the Lamb Shift in hydrogen-like U^{91+}. By increasing the temperature stability of the cryostat, even an energy resolution of $\Delta E_{\mathrm{FWHM}} = 27$ eV or below may be achieved [77].

Recently, our first two-dimensional detector array *maXs-30* with 64 microcalorimeters has been employed [78]. On the left-hand side of Figure 8, a photographic image of the detector chip consisting of 64 pixels with a total active detection area of 16 mm^2 is shown. With a nominal absorber thickness of 30 µm, a quantum efficiency above 30% is achieved for X-ray energies up to 50 keV as well as between 80 keV and 90 keV. On the right-hand side of Figure 8, an energy resolution of $\Delta E_{\mathrm{FWHM}} = 22$ eV for the 60 keV γ-line of ^{241}Am is demonstrated. As this measurement was suffering from temperature instabilities and a persistent current that was smaller than optimal, the expected energy resolution of below 6 eV could not be achieved.

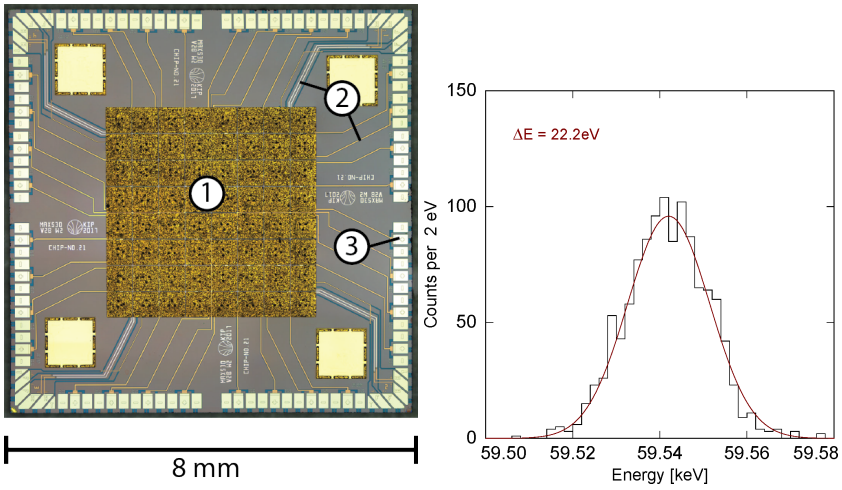

Figure 8. (color online) On the left-hand side, a microscopic image of the *maXs-30* detector chip with 64 absorbers (1) is shown. The temperature sensors as well as the read-out coil are hidden underneath the absorbers. Also marked are the connecting lines (2) for the signal read-out and the preparation of the persistent current, as well as the bonding pads (3). On the right-hand side, an example spectrum of the 60 keV γ-line of ^{241}Am is shown, taken with the *maXs-30* detector with an energy resolution of $\Delta E_{\mathrm{FWHM}} = 22$ eV.

2.3.3. Cryogenic Setup

All three detector arrays may be operated at the end of a 40 cm long side arm with an outer diameter of 80 mm in a dry dilution refrigerator [1] that is depicted on the left-hand side of Figure 9. The temperature that can be achieved at the end of this side arm is below 20 mK and offers good conditions to operate magnetic calorimeters. By using a dry cooling system, the need of refilling liquid nitrogen or liquid helium during detector operation is omitted and a continuous usage of available beam time can be achieved. Compared to our first test experiment at the ESR, where 70% of the available beam time was used for measurements [77], during our last ESR beam time duty cycles of almost 100% could be achieved.

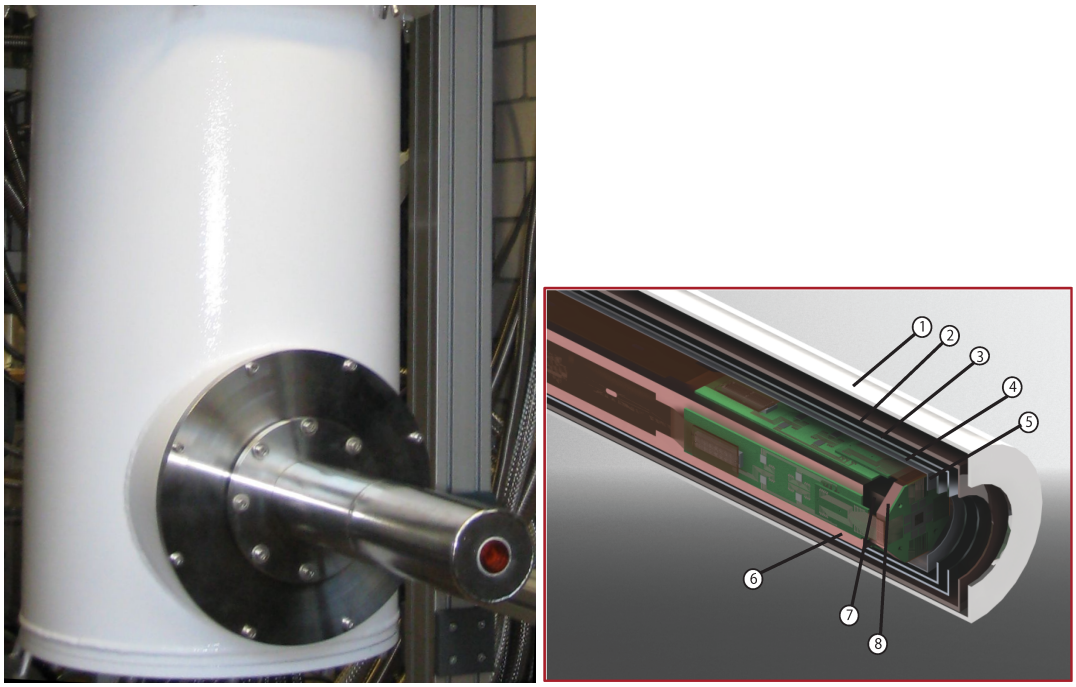

Figure 9. (color online) Photograph and schematic drawing of the side arm on which the *maXs* detector arrays can be mounted. The detector arrays are attached directly to a copper platform (8) that is mounted on a copper side arm (6 and 7). Several radiation shields (2–4) as well as two magnetic shields made of niobium (5) and μ-metal (1) enclose the inner arm.

As magnetic calorimeters are sensitive to fluctuating magnetic fields by their detection principle, disturbances by external magnetic fields might degenerate the performance of the detectors. To reduce the influence of such fields, the vacuum shield of the side arm is made of a magnetically soft, high permeability material. Closer to the detector, two additional superconducting shields made of aluminium and niobium are present at temperature stages around 800 mK and 20 mK, giving additional shielding from external fields due to the Meissner effect. Any remaining fluctuations of external fields are then further suppressed by the gradiometric design of the detectors as well as of the SQUID magnetometers. External X-ray sources can irradiate the detector through an X-ray window made of 25 µm thin beryllium and a few thin aluminium-coated mylar foils. Together, they provide a transmission larger than 80% for X-rays above 3 keV.

---

[1] BlueFors LD-250; BlueFors Cryogenics Oy Ltd, 00370 Helsinki, Finland

3. Application in Experiments at the ESR

3.1. Experimental Procedure

As mentioned in Section 1, the ions in the ESR are decelerated to the desired experimental energy, cooled and stored for seconds to minutes. In the experiments presented in this section, the ions interacted with the interal gas-jet target of the ESR [63]. With a certain probability, a bare ion captures an electron and promptly emits Lyman-α X-rays. The microcalorimeters were mounted under different observation angles at viewports provided at the gas-jet interaction chamber. The silicon microcalorimeters were mounted under an observation angle of about 135°, the magnetic microcalorimeters under 60° and 90°, respectively.

3.2. First Application of Silicon Microcalorimeters

3.2.1. First Measurement at the ESR

Figure 10 displays the spectrum of hydrogen-like uranium ions at an ion energy of 89 MeV/u, taken at the ESR as a proof of principle for the Lamb Shift experiments which are discussed in the next section [61,79]. The energy resolution of 115 eV is mostly limited by the so-called Doppler broadening. The finite diameter of the ion beam as well as of the gas jet of the target lead to a finite size of the interaction region of which the X-rays are emitted. The resulting observation under a range of emission angles is associated with a range of Doppler shifts. This means that a single X-ray energy in the emitter frame is observed as a range of X-ray energies in the laboratory frame. This again results in a broadening of the observed X-ray lines which is independent of the detector performance [61].

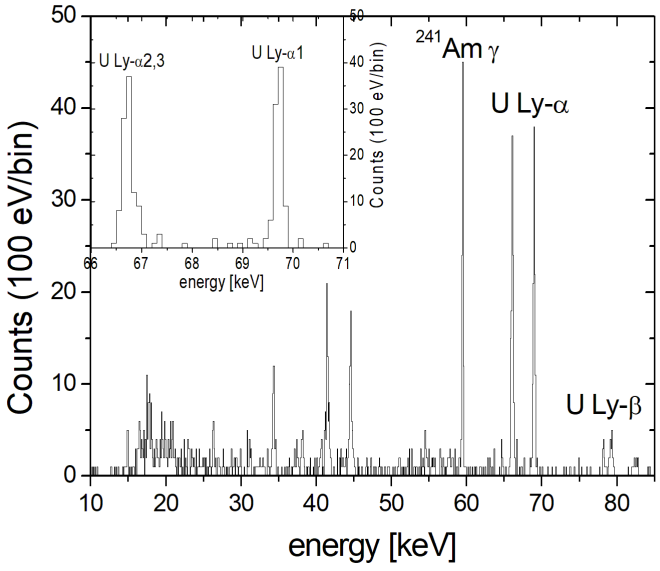

Figure 10. This example spectrum displays the Lyman-α transitions of hydrogen-like uranium U^{91+}, observed at the ESR. In this spectrum, the full width half maximum of the Lyman-α1 transition was 115 eV, limited by the so-called Doppler broadening [61,79].

3.2.2. Determination of the 1s Lamb Shift on Hydrogen-Like Lead and Gold Ions

With this excellent performance, two detector arrays with effective areas of 1.5 mm^2 and 4.2 mm^2 were applied at the ESR in two experiments to determine the 1s Lamb Shift in hydrogen-like lead and gold [61,79–81]. Figure 11 shows example spectra of Lyman-α X-rays from lead and gold ions together with calibration lines [61]. Even though the detector performance under the experimental conditions

at the ESR was sightly worse with an average energy resolution of around 200 eV, the statistical error in both cases was small compared to the systematic uncertainties.

The nonlinear energy response function of the silicon thermistors was modeled by a third order polynomial using several calibration lines (see [61] for a detailed discussion). Its contribution to the systematic uncertainty was 15%. The systematic uncertainties were dominated by the correction of the Doppler shift. In comparison to an ion trap, the ions in a storage ring have high ion energies up to several hundred MeV/u. As a consequence, the emitted X-ray lines are Doppler shifted according to the formula

$$E_{lab} = E_{emit} \cdot \frac{\sqrt{1-\beta^2}}{1-\beta\cos(\theta)}, \tag{3}$$

where β is the ion velocity and θ is the angle of observation. It is obvious that the precision of these variables ultimately will limit the accuracy in the determination of the X-ray energy. In our experiments, the main systematic limitation was introduced by the determination of θ [61]. It limited the accuracy of the Lamb Shift to about 25%. Within these error bars, the results for the 1s Lamb Shift of (260 ± 53) eV for lead and (211 ± 42) eV for gold are in good agreement with predictions from quantum electrodynamics [61]. For lead, the measurement even represents the most precise measurement of the 1s Lamb Shift to our knowledge.

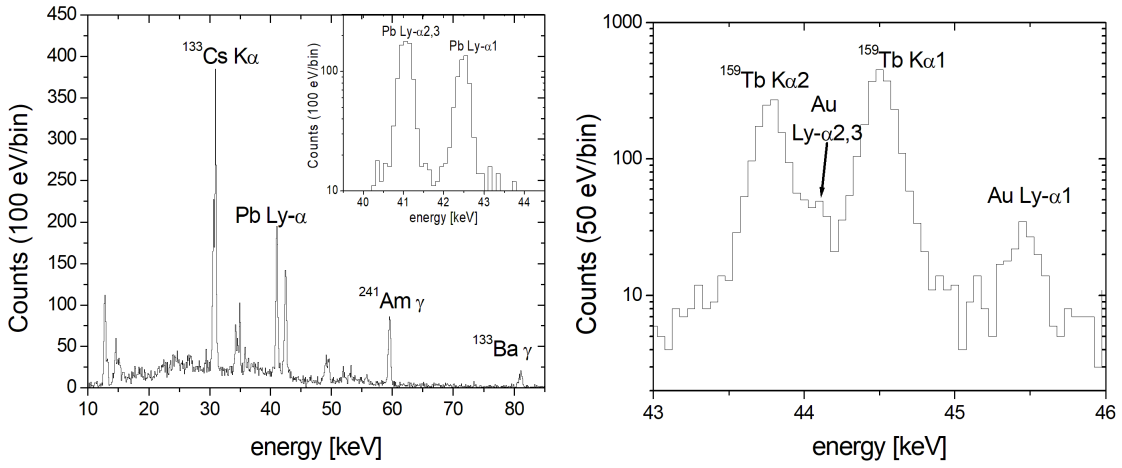

Figure 11. Two example spectra of Lyman-α X-rays from lead and gold ions together with calibration lines are displayed [61]. The spectra are not yet corrected for the Doppler shift.

3.2.3. First Tests for SiM-X

After the new pulse-tube-cooled cryostat was commissioned in the laboratory, it was for the first time applied at the ESR in a test experiment on hydrogen-like xenon using the detector array which was used in the Lamb Shift experiment [60,61]. While the cryostat with liquid nitrogen and liquid helium, which was used before in the Lamb Shift experiments, had always suffered from instabilities of the operating temperature which had to be corrected offline [81], the new cryostat maintained an excellent temperature stability over several days, which allowed for measuring X-rays with a very small count rate of 1×10^{-3} Hz. Figure 12 shows an example spectrum with the Kα and Kβ lines as well as the line of K-shell Radiative Recombination (K-REC), respectively.

The test experiment took advantage of X-rays emitted when the circulating xenon ions interacted with a hydrogen target. In principle, the comparison of our experimental values with the high-precision measurement of Thorn et al. in [53] allows for an intrinsic determination of the Doppler correction factor without the need to know specific parameters like ion beam energy or observation angle. Due to the low statistics, the determination of the K-α transition energies in our experiment is only possible with a precision of about 2% which would of course not be sufficient for a high-precision measurement.

However, the concept of intrinsic determination of the Doppler correction factor is another advantage of the large dynamic range of microcalorimeters.

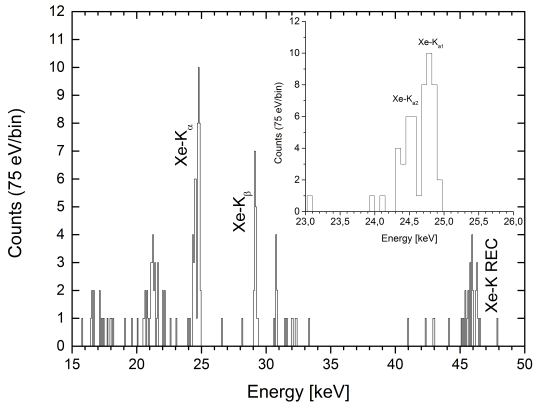

Figure 12. A spectrum of X-ray lines from hydrogen-like xenon ions interacting with a hydrogen target is displayed. The relatively small beam energy of 30.85 MeV/u resulted in a short lifetime of the beam, which in turn resulted in a rather small count rate [66]. The energy resolution in this experiment was of the order of $\Delta E \approx 180$ eV.

3.3. First Tests of Magnetic Calorimeters at the ESR

The detector arrays *maXs-200* and *maXs-30* have been operated in first experiments at the ESR during three beam times to investigate the operation of magnetic calorimeters in the environment of a storage ring [78]. In the experiments, no degradation of detector performance due to external magnetic fields was encountered. In Figure 13, a spectrum is shown that has been taken with two pixels of a *maXs-200* detector array at the gas-jet target of the ESR as an incident beam of bare Xe^{54+} ions at a beam energy of 50 MeV/u was crossing a gas jet of neutral Xe atoms [77].

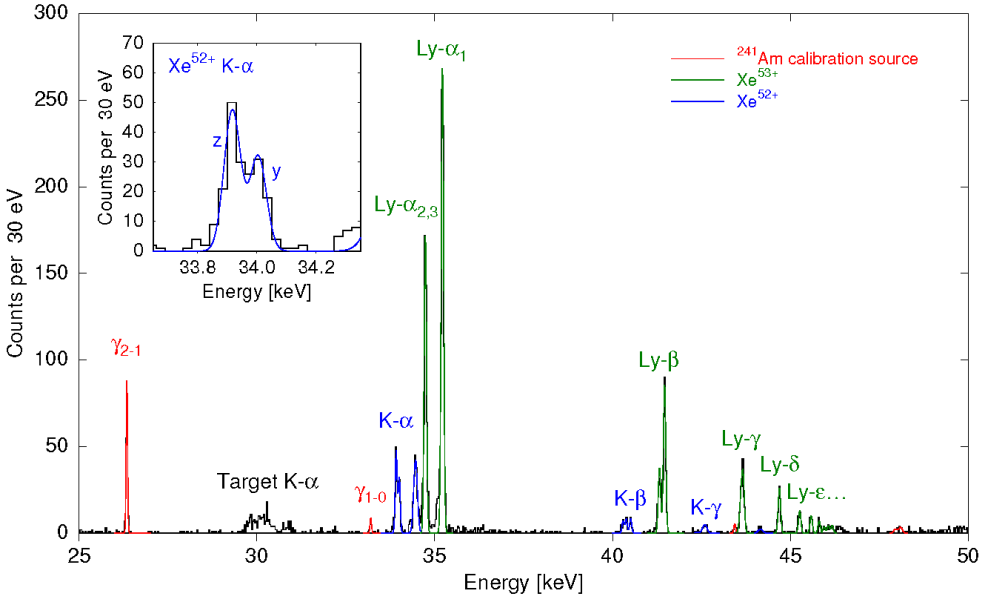

Figure 13. Lyman series of hydrogen-like Xe^{53+} up to Ly-η and the K-α and K-β lines of helium-like Xe^{52+}. The inset shows the z/y-doublet of He-like Xe^{52+}. The energy is given in the laboratory frame [77].

During the subsequent electron capture processes, X-ray photons from hydrogen-like and helium-like xenon were emitted and detected with an energy resolution of around 50 eV. The Lyman series of Xe^{53+} up to Ly-η could be observed and the line splitting of the Ly-α as well as of the Ly-β doublets could be clearly resolved. The corresponding Balmer lines at energies below 10 keV were absorbed by almost 2 m of air between the gas target and the detector and could, therefore, not be detected. However, the good energy resolution allowed for separating the z/y-doublet originating from helium-like Xe^{52+} ions as were also observed in previous measurements by Thorn et al. [53]. Due to the necessary Doppler correction, the absolute determination of the corresponding transition energies was, however, limited by the available precision of the observation angle. Therefore, an intrinsic Doppler correction was performed by calculating the Doppler shift from the Lyman-α_1 line of hydrogen-like Xe^{53+} with respect to the theoretical value of 31,283.77 eV [4]. The resulting energies for the z-line of $(30,128.2 \pm 1.2)$ eV as well as for the y-line of $(30,205.4 \pm 2.0)$ eV are in excellent agreement with theory [82] and the experiment of Thorn et al. The stated errors only include the fitting error. Uncertainties due to the Doppler correction are expected to be around 1 eV, given by the uncertainty of the determination of the line centroid of the Lyman-α_1 line. Due to a very good linearity of the detector, future experiments with ions at reduced beam energies at CRYRING will, therefore, allow for high-precision determination of absolute transition energies of highly charged ions.

The main aim of the most recent beam time was to increase the active detection area by using the newly developed two-dimensional detector array *maXs-30* and to further improve the energy resolution. On the left-hand side of Figure 14, the experimental setup consisting of one *maXs-30* chip surrounded by eight SQUID chips, each equipped with four single SQUID magnetometers that were fabricated in our cleanroom [83], is depicted.

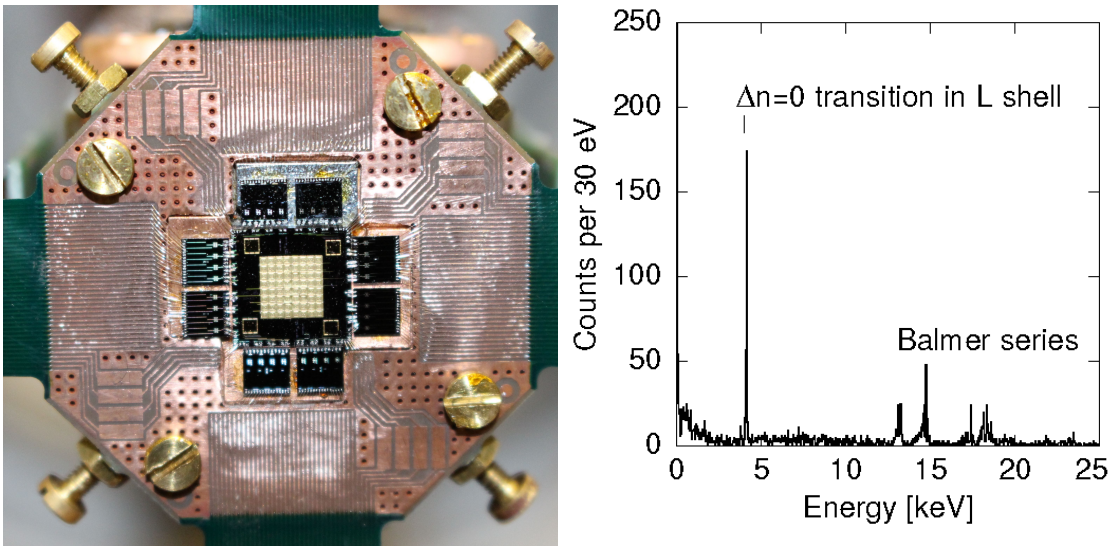

Figure 14. (color online) Detector setup comprising a *maXs-30* detector array surrounded by eight home-made SQUID chips containing four SQUID magnetometers each. On the right-hand side the Balmer series and an intra shell transition originating from a collision of lithium-like U^{89+} with a N_2 gas target that has been measured during 47 h with the *maXs-30* detector array is shown.

More than 40 pixels of the *maXs-30* detector were operated, resulting in an active detection area of more than 10 mm^2, which is five times larger than the one in our previous experiment with the *maXs-200* detector. The increased area together with the very low dark count rate of metallic magnetic calorimeters enables the detection of lines with small intensities. With this setup, a measurement at the ESR was performed over 47 h where lithium-like U^{89+} ions at 75 MeV/u interacted with a N_2 gas target. To decrease the absorption of low energy photons in air on their way to the detector that was placed in a distance of 1.3 m from the interaction chamber, a tube filled with helium was inserted in the

space between the gas-jet target and the detector. The resulting spectrum is depicted on the right-hand side of Figure 14 and shows the Balmer series above 10 keV as well as an intra shell transition of the L shell around 4 keV.

3.4. Next-Generation Detector Arrays

Besides ongoing developments to improve the signal height by increasing the persistent currents needed to operate the detectors, currently new SQUID magnetometers are produced in our cleanroom that feature promising read-out noise levels. Together with improvements in temperature stabilization, even better energy resolution should be possible in upcoming experiments. To further increase the active detection area, new read-out schemes as well as multiplexing techniques [84–86] are currently developed.

4. Conclusions and Perspectives

Microcalorimeters are versatile instruments for high-precision X-ray spectroscopy of highly charged heavy ions produced at ion storage rings. In particular, at the GSI Helmholtz Centre for Heavy Ion Research, microcalorimeters based on silicon thermistors and based on metallic magnetic calorimeters have been developed and applied at the Experimental Storage Ring (ESR). Both setups demonstrated excellent energy resolution with calibration X-ray sources and in several tests at the ESR [77]. With silicon microcalorimeters, two experiments to determine the 1s Lamb Shift on hydrogen-like lead and gold have been performed. The results of (260 ± 53) eV and (211 ± 42) eV are in good agreement with quantum electrodynamics calculations [61]. The accuracy is currently limited by the correction of the Doppler shift, which was necessary due to the high ion energies at the ESR.

There are several approaches to improve this accuracy. The first approach is to perform the experiment not at the gas-jet target but at the ESR electron cooler, where one can take advantage of measuring under 0° or 180°. Indeed, the most precise measurements for the 1s Lamb Shift on hydrogen-like ions up to now where obtained when applying germanium detectors in this geometry [19,87,88]. On the other hand, the application of microcalorimeters in this geometry has been impeded up to now by the size of the cryostat and the use of liquid helium and nitrogen. However, the next generation of microcalorimeters will be operated in a dry cryostat which is much smaller and more versatile [77,89]. With these cryostats, mounting the microcalorimeters at the electron cooler will be possible.

As a second approach, the velocity of the ions can be reduced by deceleration, thus reducing the Doppler shift and, accordingly, the systematic error connected to its correction. The ESR itself provides the opportunity to slow down heavy, highly charged ions to energies around 4 MeV/u. Unfortunately, despite the excellent vacuum in this storage ring, the lifetime of very heavy ions becomes very small at such low ion energies. At GSI, the low-energy storage ring CRYRING [20,90] as well as the heavy ion trap facility HITRAP [21,22] are currently under commissioning to solve this problem and realize the storage of heavy ions down to below 1 MeV/u at the CRYRING and of ions practically at rest in the HITRAP. When combining these facilities with the excellent performance of microcalorimeters, a considerable improvement of the accuracy for the Lamb Shift and other X-ray spectroscopy experiments can be expected.

The third approach is independent of alterations of the experimental setup. It makes use of the large dynamic range of microcalorimeters. Next to the Lyman X-ray lines, Balmer lines at energies 15–25 keV in the emitter frame are also emitted [91]. The QED corrections on these lines are negligibly small. Therefore, if they are detected in parallel to the Lyman lines, their energy can be used to determine the Doppler correction factor without detailed knowledge about the angle or the ion velocity. In our measurements with silicon micrcalorimeters on the 1s Lamb Shift, it was found that the sensitivity of the pixels, which are optimized for energies around 70 keV, was not sufficient for a reliable determination of the Doppler shift with this method. In the next generation microcalorimeters, some pixels of the arrays will be equipped with thinner absorbers optimized for energies below 10 keV,

which will then be used to determine the Doppler correction. On the other hand, metallic magnetic microcalorimeters have already demonstrated the possibility to simultaneously measure X-rays with energies in the range from 4 to 60 keV with good energy resolution. Accordingly, the application for the determination of the Doppler correction factor is possible and will be applied in experiments in the future.

The future research facility FAIR [24] will provide high-intensity beams of rare nuclides, for which high-precision X-ray spectroscopy will be an interesting subject in itself. In addition, once the Lamb Shift has been determined in stable isotopes with sufficient accuracy, the investigation of nuclear charge radii by means of the finite size contribution to the 1s Lamb Shift will be a particularly interesting subject [26,64], especially for rare or unstable nuclides.

Author Contributions: P.E. and S.K.-B. were responsible for the silicon microcalorimeters. C.E., A.F., D.H. and M.K. were responsible for the metallic magnetic calorimeters. T.S., as the head of the Atomic Physics Dept. of GSI, coordinated the experiments at the ESR and the developments for FAIR regarding storage ring physics.

Funding: This work is supported by the German Research Council via the Emmy-Noether Grant KR3721/1, and the German Ministry of Education and Research via Grants 05P15RGFAA and 05P12VHFA5.

Acknowledgments: We thank the accelerator crew of GSI, in particular the operators of the ESR, for their support during our various beam times. Discussions with H.-J. Kluge, S. Trotsenko, T. Gassner, A. Gumberidze and R. Schuch are gratefully acknowledged.

Conflicts of Interest: The authors declare no conflict of interest.

Abbreviations

The following abbreviations are used in this manuscript:

GSI	GSI Helmholtz Centre for Heavy Ion Research
ESR	Experimental Storage Ring

References

1. Porter, F.S.; Beck, B.R.; Beiersdorfer, P.; Boyce, K.R.; Brown, G.V.; Chen, H.; Gygax, J.; Kahn, S.M.; Kelley, R.L.; Kilbourne, C.A.; et al. The XRS microcalorimeter spectrometer at the Livermore electron beam ion trap. *Can. J. Phys.* **2008**, *86*, 231–240.
2. Lamb, W.E.; Retherford, R.C. Fine structure of the hydrogen atom by a microwave method. *Phys. Rev.* **1947**, *72*, 241, doi:10.1103/PhysRev.72.241.
3. Niering, M.; Holzwarth, R.; Reichert, J.; Pokasov, P.; Udem, T.; Weitz, M.; Hänsch, T.W.; Lemonde, P.; Santarelli, G.; Abgrall, M.; et al. Measurement of the hydrogen 1S–2S transition frequency by phase coherent comparison with a microwave cesium fountain clock. *Phys. Rev. Lett.* **2000**, *84*, 5496, doi:10.1103/PhysRevLett.84.5496.
4. Johnson, W.R.; Soff, G. The Lamb shift in hydrogen-like Atoms, $1 \leq Z \leq 110$. *Atom. Data Nucl. Data Tab.* **1985**, *33*, 405.
5. Beier, T.; Mohr, P.; Persson, H.; Plunien, G.; Greiner, M.; Soff, G. Current status of Lamb shift predictions for heavy hydrogen-like ions. *Phys. Lett. A* **1997**, *236*, 329–338.
6. Yerokhin, V.A.; Shabaev, V.M. Lamb shift of n = 1 and n = 2 states of hydrogen-like atoms, $1 \leq Z \leq 110$. *J. Phys. Chem. Ref. Data* **2015**, *44*, 033103, doi:10.1063/1.4927487.
7. Stöhlker, T.; Gumberidze, A.; Trassinelli, M.; Andrianov, V.; Beyer, H.F.; Kraft-Bermuth, S.; Bleile, A.; Egelhof, P.; The FOCAL collaboration. Quantum electrodynamics in extreme fields: Precision spectroscopy of high-Z H-like systems. *Lect. Notes Phys.* **2008**, *745*, 157–163.
8. Beiersdorfer, P. Precision energy-level measurements and QED of highly charged ions. *Can. J. Phys.* **2009**, *87*, 9–14.
9. Beiersdorfer, P. Testing QED and atomic-nuclear interactions with high-Z ions. *J. Phys. B* **2010**, *43*, 074032.
10. Kubicek, K.; Mokler, P.H.; Mäckel, V.; Ullrich, J.; Lopez-Urrutia, J.R.C. Transition energy measureemnts in hydrogenlike and heliumlike ions strongly supporting bound-state QED calculations. *Phys. Rev. A* **2014**, *90*, 032508,

11. Beiersdorfer, P.; Britten, J.A.; Brown, G.V.; Chen, H.; Clothiaux, E.J.; Cottam, J.; Förster, E.; Gu, M.F.; Harris, C.L.; Kahn, S.M.; et al. Current research with highly charged ions in EBIT-II and SuperEBIT. *Phys. Scr. T* **2001**, *92*, 268, doi:10.1238/Physica.Topical.092a00268.
12. Beiersdorfer, P. A "brief" history of spectroscopy on EBIT. *Can. J. Phys.* **2008**, *86*, 1–10.
13. Beiersdorfer, P. Highly charged ions in magnetic fusion plasmas: research opportunities and diagnostic necessities. *J. Phys. B* **2010**, *48*, 144017, doi:10.1088/0953-4075/48/14/144017.
14. McDonald, J.W.; Bauer, R.W.; Schneider, D.H.G. Extraction of highly charged ions (up to 90+) from a high-energy electron-beam ion trap. *Rev. Sci. Instrum.* **2002**, *73*, 30–35.
15. Beiersdorfer, P.; Chen, H.; Thorn, D.B.; Träbert, E. Measurement of the two-loop Lamb Shift in lithiumlike U^{89+}. *Phys. Rev. Lett.* **2005**, *95*, 233003, doi:10.1103/PhysRevLett.95.233003.
16. Schweikhard, L.; Beiersdorfer, P.; Brown, G.V.; Lupez-Urrutia, J.R.C.; Utter, S.B.; Widmann, K. Pulsed gas injection for X-ray spectroscopy of highly charged ions stored in the magnetic trapping mode of an electron beam ion trap. *Nucl. Instrum. Methods B* **1998**, *142*, 245–252.
17. Marrs, R.E.; Elliot, S.R.; Knapp, D.A. Production and trapping of hydrogenlike and bare uranium ions in an electron beam ion trap. *Phys. Rev. Lett.* **1994**, *72*, 4082, doi:10.1103/PhysRevLett.72.4082.
18. Eichler, J.; Stöhlker, T. Radiative electron capture in relativistic ion-atom collisions and the photoelectric effect in hydrogen-like high-Z systems. *Phys. Rep.* **2007**, *439*, 1–99.
19. Gumberidze, A.; Stöhlker, T.; Banas, D.; Beckert, K.; Beller, P.; Beyer, H.F.; Bosch, F.; Hagmann, S.; Kozhuharov, C.; Liesen, D.; et al. Quantum electrodynamics in strong electric fields: The ground-state Lamb shift in hydrogenlike uranium. *Phys. Rev. Lett.* **2005**, *94*, 223001.
20. Lestinsky, M.; Litvinov, Y. Physics book: CRYRING@ESR. *Eur. Phys. J. Spec. Top.* **2016**, *225*, 797–882.
21. Kluge, H.J.; Quint, W.; Winters, D.F.A. Atomic physics experiments with trapped and cooled highly charged ions. *J. Phys. Conf. Ser.* **2007**, *58*, 9, doi:10.1088/1742-6596/58/1/002.
22. Herfurth, F.; Andelkovic, Z.; Barth, W.; Chen, W.; Dahl, L.A.; Fedotova, S.; Gerhard, P.; Kaiser, M.; Kester, O.K.; Kluge, H.J.; et al. The HITRAP facility for slow highly charged ions. *Phys. Scr.* **2015**, *166*, 014065, doi:10.1088/0031-8949/2015/T166/014065.
23. Geissel, H.; Armbruster, P.; Behr, K.H.; Brünle, A.; Burkard, K.; Cheng, M.; Folger, H.; Franczak, B.; Keller, H.; Klepper, O.; et al. The GSI projectile fragment separator (FRS): a versatile magnetic system for relativistic ions. *Nucl. Instrum. Methods B* **1992**, *70*, 286–297.
24. Facility for Antiproton and Ion Research in Europe GmbH (FAIR). Available online: www.fair-center.de (accessed on 26 October 2018).
25. Stöhlker, T.; Litvinov, Y.A.; for the SPARC Collaboration. Atomic physics experiments at the high energy storage ring. *Phys. Scr. T* **2015**, *166*, 014025.
26. Stöhlker, T.; Bagnoud, V.; Blaum, K.; Blazevic, A.; Bräuning-Demian, A.; Durante, M.; Herfurth, F.; Lestinsky, M.; Litvinov, Y.; Nevv, S.; et al. APPA at FAIR: From fundamental to applied research. *Nucl. Instrum. Methods B* **2015**, *365*, 680–685.
27. Tashenov, S.; Banas, D.; Beyer, H.; Brandau, C.; Fritzsche, S.; Gumberidze, A.; Hagmann, S.; Hillenbrand, P.M.; Jörg, H.; Kozhuharov, I.; et al. Observation of coherence in the time-reversed relativistic photoelectric effect. *Phys. Rev. Lett.* **2014**, *113*, 113001, doi:10.1103/PhysRevLett.113.113001.
28. Lopez-Urrutia, J.R.C.; Artemyev, A.; Braun, J.; Brenner, G.; Bruhns, H.; Draganic, I.N.; Martinez, A.J.G.; Lapierre, A.; Mironov, V.; Scofield, J.; et al. High precision measurements of forbidden transitions in highly charged ions at the Heidelberg EBIT. *Nucl. Instrum. Methods B* **2005**, *235*, 85–91.
29. Lapierre, A.; Lopez-Urrutia, J.R.C.; Baumann, T.M.; Epp, S.W.; Gonchar, A.; Gonzalez-Martinez, A.J.; Liang, G.; Rohr, A.; Orts, R.S.; Simon, M.C.; et al. Compact soft x-ray spectrometer for plasma diagnostics at the Heidelberg Electron Beam Ion Trap. *Rev. Sci. Instrum.* **2007**, *78*, 123105, doi:10.1063/1.2818808.
30. Biedermann, C.; Radtke, R.; Seidel, R.; Pütterich, T. Spectroscopy of highly charged tungsten ions relevant for fusion plasmas. *Phys. Scr. T* **2009**, *134*, 014026, doi:10.1088/0031-8949/2009/T134/014026.
31. Amaro, P.; Szabo, C.I.; Schlesser, S.; Gumberidze, A.E.K., Jr.; Henins, A.; Bigot, E.O.L.; Trassinelli, M.; Isac, J.M.; Travers, P.; Guerra, M.; et al. A vacuum double-crystal spectrometer for reference-free X-ray spectroscopy of highly charged ions. *Radiat. Phys. Chem.* **2014**, *98*, 132–149.

32. Beyer, H.; Gassner, T.; Trassinelli, M.; Heß, R.; Spillmann, U.; Banas, D.; Blumenhagen, K.H.; Bosch, F.; Brandau, C.; Chen, W.; et al. Crystal optics for precision X-ray spectroscopy on highly-charged ions—Conception and proof. *J. Phys. B* **2015**, *48*, 144010.
33. Uhlig, J.; Doriese, W.B.; Fowler, J.W.; Swetz, D.S.; Jaye, C.; Fischer, D.A.; Reintsema, C.D.; Bennett, D.A.; Vale, L.R.; Mandal, U.; et al. High-resolution X-ray emission spectroscopy with transition-edge sensors: Present performance and future potential. *J. Synchrotron Radiat.* **2015**, *22*, 766–775.
34. Egelhof, P.; Beyer, H.F.; McCammon, D.; v. Felitzsch, F.; v. Kienlin, A.; Kluge, H.J.; Liesen, D.; Meier, J.; Moseley, S.H.; Stöhlker, T. Application of low temperature calorimeters for precise Lamb shift measurements in hydrogen-like very heavy ions. *Nucl. Instrum. Methods A* **1996**, *370*, 263–265.
35. Silver, E.; Schnopper, H.; Austin, G.; Ingram, R.; Guth, G.; Murray, S.; Madden, N.; Landis, D.; Beeman, J.; Haller, E.E.; et al. Using a microcalorimeter to measure the Lamb shift in hydrogenic gold and uranium on cooled, decelerated ion beams. *Nucl. Instrum. Methods A* **2004**, *520*, 60–62.
36. Mazin, B.A.; Bumble, B.; Day, P.K.; Eckart, M.E.; Golwala, S.; Zmuidzinas, J.; Harrison, F.A. Position sensitive x-ray spectrophotometer using microwave kinetic inductance detectors. *Appl. Phys. Lett.* **2006**, *89*, 222507, doi:10.1063/1.2390664.
37. Ulbricht, G.; Mazin, B.A.; Szypryt, P.; Walter, A.B.; Bockstiegel, C.; Bumble, B. High multiplexible thermal kinetic inductance detectors for x-ray imaging spectroscopy. *Appl. Phys. Lett.* **2015**, *106*, 251103, doi:10.1063/1.4923096.
38. Friedrich, S.; Segall, K.; Gaidis, M.C.; Wilson, C.M.; Prober, D.E.; Szymkowiak, A.E.; Moseley, S.H. Experimental quasiparticle dynamics in a superconducting, imaging x-ray spectrometer. *Appl. Phys. Lett.* **1997**, *71*, 3901–3903.
39. Friedrich, S. Superconducting tunnel junction photon detectors: Theory and Applications. *J. Low Temp. Phys.* **2008**, *151*, 277–286.
40. Enss, C. (Ed.) *Cryogenic Particle Detection*; Topics in Applied Physics Book Series; Springer: Berlin/Heidelberg, Germany, 2005; Volume 99.
41. Camus, P.; Julliard, A. Low Temperature Detectors LTD-16. *J. Low Temp. Phys.* **2015**, *185*, 173706.
42. Doriese, W.B.; Abbamonte, P.; Alpert, B.K.; Bennett, D.A.; Denison, E.V.; Fang, Y.; Fischer, D.A.; Fitzgerald, C.P.; Fowler, J.W.; Gard, J.D.; et al. A practical superconducting-microcalorimeter X-ray spectrometer for beamline and laboratory science. *Rev. Sci. Instrum.* **2017**, *88*, 053108, doi:10.1063/1.4983316.
43. Ullom, J.N.; Bennett, D.A. Review of superconducting transition-edge sensors for x-ray and gamma-ray spectroscopy. *Supercond. Sci. Technol.* **2015**, *28*, 084003, doi:10.1088/0953-2048/28/8/084003.
44. Mott, N.F. Conduction in non-crystalline materials. *Philos. Mag.* **1969**, *19*, 835.
45. Stahle, C.; Kelley, R.L.; McCammon, D.; Moseley, S.H.; Szymkowiak, A.E. Microcalorimeter arrays for high resolution soft X-ray spectroscopy. *Nucl. Instrum. Methods A* **1996**, *370*, 173–176.
46. McCammon, D.; Almy, R.; Apodaca, E.; Tiest, W.B.; Cui, W.; Deiker, S.; Galeazzi, M.; Juda, M.; Lesser, A.; Mihara, T.; et al. A high spectral resolution observation of the soft x-ray diffusive background with thermal detectors. *Astrophys. J.* **2002**, *576*, 188, doi:10.1086/341727.
47. Porter, F.S.; Brown, G.V.; Cottam, J. X-Ray Astronomy and Astrophysics. In *Cryogenic Particle Detection*; Topics in Applied Physics Book Series, Volume 99; Springer: Berlin/Heidelberg, Germany, 2005.
48. Hitomi Collaboration; Aharonian, F. The Quiescent Intracluster Medium in the Core of the Perseus Cluster. *Nature* **2016**, *535*, 117–121.
49. Porter, F.S.; Brown, G.V.; Boyce, K.R.; Kelley, R.L.; Kilbourne, C.A.; Beiersdorfer, P.; Chen, H.; Terracol, S.; Kahn, S.M.; Symkowiak, A.E. The Astro-E2 X-ray spectometer/EBIT microcalorimeter x-ray spectrometer. *Rev. Sci. Instrum.* **2004**, *75*, 3772, doi:10.1038/nature18627.
50. Porter, F.S.; Beiersdorfer, P.; Brown, G.V.; Doriese, W.; Gygax, J.; Kelley, R.L.; Kilbourne, C.A.; King, J.; Irwin, K.; Reintsema, C.; et al. The EBIT calorimeter spectrometer: A new, permanent user facility at the LLNL EBIT. *J. Low Temp. Phys.* **2008**, *151*, 1061–1066.
51. Hell, N.; Brown, G.V.; Wilms, J.; Grinberg, V.; Clementson, J.; Liedahl, D.; Porter, F.S.; Kelley, R.L.; Kilbourne, C.A.; Beiersdorfer, P. Laboratory measurements of the K-shell transition energies in L-shell ions of Si and S. *Astrophys. J.* **2016**, *830*, 26, doi:10.3847/0004-637X/830/1/26.
52. Panchenko, D.; Beiersdorfer, P.; Hell, N.; Brown, G.V.; Kelley, R.; Kilbourne, C.A.; Porter, F.S. Resonance-to-intercombination-line ratios of neonlike ions in the relativistic regime. *Phys. Rev. A* **2017**, *95*, 062503, doi:10.1103/PhysRevA.95.062503.

53. Thorn, D.B.; Gu, M.F.; Brown, G.V.; Beiersdorfer, P.; Porter, F.S.; Kilbourne, C.A.; Kelley, R.L. Precision measurement of the K-shell spectrum from highly-charged xenon with an array of X-ray calorimeters. *Phys. Rev. Lett.* **2009**, *103*, 163001.
54. Thorn, D.B.; Brown, G.V.; Clementson, J.H.; Chen, H.; Chen, M.; Beiersdorfer, P.; Boyce, K.R.; Kilbourne, C.A.; Porter, F.S.; Kelley, R.L. High-resolution spectroscopy of K-shell praseodymium with a high-energy microcalorimeter. *Can. J. Phys.* **2008**, *86*, 241–244.
55. Clementson, J.; Beiersdorfer, P.; Brown, G.V.; Gu, M.F.; Lundberg, H.; Podpaly, Y.; Träbert, E. Tungsten spectroscopy at the Livermore electron beam ion trap facility. *Can. J. Phys.* **2011**, *89*, 571–580.
56. Beck, B.R.; Becker, J.A.; Beiersdorfer, P.; Brown, G.V.; Moody, K.J.; Wilhelmy, J.B.; Porter, F.S.; Kilbourne, C.A.; Kelley, R.L. Energy splitting of the ground state doublet in the nucleus ^{229}Th. *Phys. Rev. Lett.* **2007**, *98*, 142501.
57. Zink, B.L.; Ullom, J.N.; Beall, J.A.; Irwin, K.D.; Doriese, W.B.; Duncan, W.D.; Ferreira, L.; Hilton, G.C.; Horansky, R.D.; Reintsema, C.D.; et al. Array-compatible transition edge sensor microcalorimeter γ-ray detector with 42 eV energy resolution at 103 keV. *Appl. Phys. Lett.* **2006**, *89*, 124101, doi:10.1063/1.2352712.
58. Doriese, W.; Ullom, J.N.; Beall, J.A.; Duncan, W.D.; Ferreira, L.; Hilton, G.C.; Horansky, R.D.; Irwin, K.D.; Mates, J.A.B.; Reintsema, C.D.; et al. 14-pixel, multiplexed array of gamma-ray microcalorimeters with 47 eV energy resolution at 103 keV. *Appl. Phys. Lett.* **2007**, *90*, 193508.
59. Bleile, A.; Egelhof, P.; Kluge, H.J.; Liebisch, U.; McCammon, D.; Meier, H.J.; Sebastian, O.; Stahle, C.K.; Weber, M. Low-temperature X-ray detectors for precise Lamb Shift measurements on hydrogen-like heavy ions. *Nucl. Instrum. Methods A* **2000**, *444*, 488–491.
60. Bleile, A.; Egelhof, P.; Kraft, S.; McCammon, D.; Meier, H.J.; Shrivastava, A.; Stahle, C.K.; Weber, M. Calorimetric low-temperature detectors for high resolution X-ray spectroscopy on stored highly stripped heavy ions. *AIP Conf. Proc.* **2002**, *605*, 409–412.
61. Kraft-Bermuth, S.; Andrianov, V.; Bleile, A.; Echler, A.; Egelhof, P.; Grabitz, P.; Ilieva, S.; Kiselev, O.; Kilbourne, C.; McCammon, D.; et al. Precise determination of the 1s Lamb Shift in hydrogen-like lead and gold ions using microcalorimeters. *J. Phys. B* **2017**, *50*, 055603.
62. Reich, H.; Bourgeois, W.; Franzke, B.; Kritzer, A.; Varentsov, V. The ESR internal target. *Nucl. Phys. A* **1997**, *626*, 417–425.
63. Kühnel, M.; Petridis, N.; Winters, D.F.A.; Popp, U.; Dörner, R.; Stöhlker, T.; Grisenti, R.E. Low-Z internal target from a cryogenically cooled liquid micorjet source. *Nucl. Instrum. Methods A* **2009**, *602*, 311–314.
64. Egelhof, P.; Kraft-Bermuth, S. Heavy ion physics. In *Cryogenic Particle Detection*; Topics in Applied Physics Book Series; Springer: Berlin/Heidelberg, Germany, 2005; Volume 99.
65. Scholz, P.A.; Kraft-Bermuth, S.; Andrianov, V. Systematic vibration studies on a cryogen-free ^{3}He/^{4}He dilution refrigerator for X-ray spectroscopy at storage rings. *J. Low Temp. Phys.* **2016**, *184*, 576–582.
66. Scholz, P.A.; Andrianov, V.; Echler, A.; Egelhof, P.; Kilbourne, C.; Kiselev, O.; Kraft-Bermuth, S.; McCammon, D. High-precision X-ray spectroscopy of highly charged ions at the Experimental Storage Ring using silicon microcalorimeters. *Nucl. Instrum. Methods B* **2017**, *408*, 323–325.
67. Bühler, M.; Umlauf, E. A magnetic bolometer for single-particle detection. *Europhys. Lett.* **1988**, *5*, 297.
68. Enss, C.; Fleischmann, A.; Horst, K.; Schönefeld, J.; Adams, J.S.; Huang, Y.H.; Kim, Y.H.; Seidel, G.M. Metallic magnetic calorimeters for particle detection. *J. Low Temp. Phys.* **2000**, *121*, 137–176.
69. Fleischmann, A.; Schönefeld, J.; Sollner, J.; Enss, C.; Adams, J.S.; Bandler, S.R.; Kim, Y.H.; Seidel, G.M. Low Temperature Properties of Erbium In Gold. *J. Low Temp. Phys.* **2000**, *118*, 7–21.
70. Bates, C.R.; Pies, C.; Kempf, S.; Hengstler, D.; Fleischmann, A.; Gastaldo, L.; Enss, C.; Friedrich, S. Reproducibility and calibration of MMC-based high-resolution gamma detectors. *Appl. Phys. Lett.* **2016**, *109*, 023513, doi:10.1063/1.4958699.
71. McCammon, D.; Cui, W.; Juda, M.; Morgenthaler, J.; Zhang, J.; Kelley, R.; Holt, S.; Madejski, G.; Moseley, S.; Szymkowiak, A. Thermal calorimeters for high resolution X-ray spectroscopy. *Nucl. Instrum. Methods* **1993**, *326*, 157–165.
72. Cosulich, E.; Gatti, F.; Vitale, S. Further results on μ-calorimeters with superconducting absorber. *J. Low Temp. Phys.* **1993**, *93*, 263–268.

73. Stahle, C.; Kelley, R.; Moseley, S.; Szymkowiak, A.; Juda, M.; McCammon, D.; Zhang, J. Delayed thermalization of X-rays absorbed in tin films far below the superconducting transition temperature. *Physica B* **1994**, *194*, 127–128.
74. Fleischmann, A.; Gastaldo, L.; Kempf, S.; Kirsch, A.; Pabinger, A.; Pies, C.; Porst, J.; Ranitzsch, P.; Schäfer, S.; v. Seggern, F.; et al. Metallic magnetic calorimeters. *AIP Conf. Proc.* **2009**, *1185*, 151–216.
75. Pies, C.; Schäfer, S.; Heuser, S.; Kempf, S.; Pabinger, A.; Porst, J.P.; Ranitsch, P.; Foerster, N.; Hengstler, D.; Kampkötter, A.; et al. maXs: Microcalorimeter Arrays for High-Resolution X-Ray Spectroscopy at GSI/FAIR. *J. Low Temp. Phys.* **2012**, *167*, 269–279.
76. Kempf, S.; Fleischmann, A.; Gastaldo, L.; Enss, C. Physics and applications of metallic magnetic calorimeters. *J. Low Temp. Phys.* **2018**, *193*, 365–379.
77. Hengstler, D.; Keller, M.; Schötz, C.; Geist, J.; Krantz, M.; Kempf, S.; Gastaldo, L.; Fleischmann, A.; Gassner, T.; Weber, G.; et al. Towards FAIR: First measurements of metallic magnetic calorimeters for high-resolution x-ray spectroscopy at GSI. *Phys. Scr.* **2015**, *2015*, 014054, doi:10.1088/0031-8949/2015/T166/014054.
78. Hengstler, D. Development and Characterization of Two-Dimensional Metallic Magnetic Calorimeter Arrays for the High-Resolution X-Ray Spectroscopy. Ph.D. Thesis, Heidelberg University, Heidelberg, Germany, 2017.
79. Andrianov, V.; Beckert, K.; Beller, P.; Bleile, A.; Egelhof, P.; Gumberidze, A.; Ilieva, S.; Kiselev, O.; Kilbourne, C.; Kluge, H.J.; et al. First experiments aiming for precise Lamb Shift measurements on hydrogen-like heavy ions with low temperature calorimeters. *J. Low Temp. Phys.* **2008**, *151*, 1049–1054.
80. Andrianov, V.; Beckert, K.; Bleile, A.; Chatterjee, C.; Echler, A.; Egelhof, P.; Gumberidze, A.; Ilieva, S.; Kiselev, O.; Kilbourne, C.; et al. Precise Lamb shift measurements in hydrogen-like heavy ions—status and perspectives. *AIP Conf. Proc.* **2009**, *1185*, 99–102.
81. Kraft-Bermuth, S.; Andrianov, V.; Bleile, A.; Echler, A.; Egelhof, P.; Grabitz, P.; Kilbourne, C.; Kiselev, O.; McCammon, D.; Scholz, P. Precise determination of the Lyman-α1 transition energy in hydrogen-like gold ions with microcalorimeters. *J. Low Temp. Phys.* **2014**, *176*, 1002–1008.
82. Plante, D.R.; Johnson, W.R.; Sapirstein, J. Relativistic all-order many body calculations of the n = 1 and n = 2 states of heliumlike ions. *Phys. Rev. A* **1994**, *49*, 3519, doi:10.1103/PhysRevA.49.3519.
83. Kempf, S.; Ferring, A.; Fleischmann, A.; Enss, C. Direct-current superconducting quantum interference devices for the readout of metallic magnetic calorimeters. *Supercond. Sci. Technol.* **2015**, *28*, 045008, doi:10.1088/0953-2048/28/4/045008.
84. Kempf, S.; Wegner, M.; Fleischmann, A.; Gastaldo, L.; Herrmann, F.; Papst, M.; Richter, D.; Enss, C. Demonstration of a scalable frequency-domain readout of metallic magnetic calorimeters by means of a microwave SQUID multiplexer. *AIP Adv.* **2017**, *7*, 015007, doi:10.1063/1.4973872.
85. Mates, J.A.B.; Becker, D.T.; Bennett, D.A.; Dober, B.J.; Gard, J.D.; Hays-Wehle, J.P.; Fowler, J.W.; Hilton, G.C.; Reintsema, C.D.; Schmidt, D.R.; et al. Simultaneous readout of 128 X-ray and gamma-ray transition-edge microcalorimeters using microwave SQUID multiplexing. *Appl. Phys. Lett.* **2017**, *111*, 062601, doi:10.1063/1.4986222.
86. Morgan, K.M.; Alpert, B.K.; Bennett, D.A.; Denison, E.V.; Doriese, W.B.; Fowler, J.W.; Gard, J.D.; Hilton, G.C.; Irwin, K.D.; Joe, Y.I.; et al. Code-division-multiplexed readout of large arrays of TES microcalorimeters. *Appl. Phys. Lett.* **2016**, *109*, 112604, doi:10.1063/1.4962636.
87. Beyer, H.; Liesen, D.; Bosch, F.; Finlayson, K.D.; Jung, M.; Klepper, O.; Moshammer, R.; Beckert, K.; Eickhoff, H.; Franzke, B.; et al. X rays from radiative electron capture of free cooling electrons for precise Lamb-shift measurements at high Z: Au^{78+}. *Phys. Lett. A* **1994**, *184*, 435–439.
88. Beyer, H.; Menzel, G.; Liesen, D.; Gallus, A.; Bosch, F.; Desplattes, R.; Indelicato, P.; Stöhlker, T.; Klepper, O.; Moshammer, R.; et al. Measurement of the ground-state Lamb shift of hydrogenlike uranium at the electron cooler of the ESR. *Z. Physik D* **1995**, *35*, 169–175.
89. Kraft-Bermuth, S.; Andrianov, V.; Bleile, A.; Echler, A.; Egelhof, P.; Ilieva, S.; Kilbourne, C.; McCammon, D.; Zhang, L. Calorimetric low-temperature detectors for X-ray spectroscopy on trapped highly-charged heavy ions. *J. Low Temp. Phys.* **2012**, *167*, 765–770.

90. Stöhlker, T.; Litvinov, Y.A.; Bräuning-Demian, A.; Lestinsky, M.; Herfurth, F.; Maier, R.; Prasuhn, D.; Schuch, R.; Steck, M.; for the SPARC Collaboration. SPARC collaboration: New strategy for storage ring physics at FAIR. *Hyperfine Interact.* **2014**, *227*, 45–53.
91. Reuschl, R.; Gumberidze, A.; Stöhlker, T.; Kozhuharov, C.; Rzadkiewicz, J.; Spillmann, U.; Tashenov, S.; Fritzsche, S.; Surzhykov, A. The Balmer spectrum of H-like uranium produced by radiative recombination at low velocities. *Radiat. Phys. Chem.* **2006**, *75*, 1740–1743.